Marine Pollution Bulletin 104 (2016) 279–289

Contents lists available at ScienceDirect

Marine Pollution Bulletin

journal homepage: www.elsevier.com/locate/marpolbul

Oil droplets transport due to irregular waves: Development of large-scale spreading coefficients

Xiaolong Geng [a], Michel C. Boufadel [a,*], Tamay Ozgokmen [b], Thomas King [c], Kenneth Lee [d], Youyu Lu [c], Lin Zhao [a]

[a] Center for Natural Resources Development and Protection, Department of Civil and Environmental Engineering, New Jersey Institute of Technology, Newark, NJ 07102, United States
[b] Department of Ocean Sciences, University of Miami, Miami, FL 33149, United States
[c] Department of Fisheries and Oceans Canada, Bedford Institute of Oceanography, Dartmouth, NS B2Y 4A2, Canada
[d] Flagship of Wealth from Oceans, Commonwealth Scientific and Industry Research Organization (CSIRO), Perth, WA 6151, Australia

ARTICLE INFO

Article history:
Received 15 May 2015
Accepted 5 January 2016
Available online 12 January 2016

Keywords:
JONSWAP
Oil spill model
Eddy diffusivity
Buoyancy
Particle tracking
Irregular waves

ABSTRACT

The movement of oil droplets due to waves and buoyancy was investigated by assuming an irregular sea state following a JONSWAP spectrum and four buoyancy values. A technique known as Wheeler stretching was used to model the movement of particles under the moving water surface. In each simulation, 500 particles were released and were tracked for a real time of 4.0 h. A Monte Carlo approach was used to obtain ensemble properties. It was found that small eddy diffusivities that decrease rapidly with depth generated the largest horizontal spreading of the plume. It was also found that large eddy diffusivities that decrease slowly with depth generated the smallest horizontal spreading coefficient of the plume. The increase in buoyancy resulted in a decrease in the horizontal spreading coefficient, which suggests that two-dimensional (horizontal) models that predict the transport of surface oil could be overestimating the spreading of oil.

1. Introduction

Waves play an important role in the transport and fate of oil spills (Sobey and Barker, 1997; Korotenko et al., 2000; Wang et al., 2005). The water velocity engendered by waves causes the shearing of the oil slick and its breakup into droplets, the smaller of which sink deeper into the water column. Understanding the effects of waves on slicks at sea has been hampered by logistical difficulty, as it is not possible to have sufficient measurements to have a predictive relation between the sea state and the oil droplet distribution in the water column. This has led to extensive wave tank studies where such relations were sought and developed (Coulaloglou and Tavlarides, 1977; Millies and Mewes, 1999; Pohorecki et al., 2001). Regardless of the success of these relations at the field scale, there are very few works that explored the effect of waves on the transport and spreading of oil droplets at sea. The vast majority of works (and the current practice) computes the bulk transport of oil based on wind direction and speed, and predicts the spreading using empirical coefficients based on the experience of the operator (ASCE Task Committee, 1996; Boufadel et al., 2014). However, there is no assurance that such values could be used at another location or even at the same location under different sea states.

Elliot et al. (1986) briefly addressed the direct effect of waves on transport. Another one Walter and Blanch (1986) used a depth averaged formulation to account for transport due to waves. Boufadel et al. (2006) and (2007) investigated the effects of regular waves on dispersed oil. They explained, among other, the "comet" shape of spills based on the droplet sizes and the Stokes drift; as the large droplet stay closer to the surface, they get entrained forward by the Stokes drift, which is maximum at the surface. The smaller droplets, thus, trail behind, giving the appearance of a comet. The current work expands on the previous work by considering irregular waves, which is more realistic. This also requires using different numerical techniques for tracking the water surface and for obtaining the velocity at the water surface. In particular, velocity values in irregular waves cannot be referred to the Mean Water Level (MWL), as the MWL is an ensemble-engendered quantity, and the water surface could be much higher or much lower than the MWL.

We assume the sea to be well represented by the empirical spectrum JONSWAP (Hasselmann et al., 1973), and particle tracking techniques was adopted within a Monte Carlo framework. We focus on analyzing the role of the turbulent diffusion in the mixed layer in affecting the spatial distribution of the oil droplets. We also treat the oil as consisting of a large number of identical particles, and we consider situations where they are buoyant.

The layout of this paper is as follows: first the fundamentals of droplet transport at sea and justification of the choice of the JONSWAP spectrum are presented. Then the details of numerical implementation are given such as the range of frequency of the JONSWAP spectrum and the cases investigated in this paper by varying buoyancy velocity and

* Corresponding author.
E-mail address: boufadel@gmail.com (M.C. Boufadel).

http://dx.doi.org/10.1016/j.marpolbul.2016.01.007
0025-326X/

eddy diffusivity. Finally, the simulation results are presented to address the roles of diffusivity and buoyancy in oil transport.

2. Methodology

2.1. JONSWAP wave spectrum

The sea state can be defined in a variety of ways. For example, one may use the Beaufort scale (Singleton, 2008) that describes the sea state based on qualitative terms. It is an empirical yet expedient scale. A more quantitative means is the wave magnitude Fourier spectrum (Phillips, 1985), which is essentially a plot of wave height as function of the corresponding wave period or wave length. The earliest work on the spectrum was reported in the seminal work of O.M. Philips (see in Phillips, 1985), who surmised that the spectrum becomes "saturated" at high wave frequency or high wave numbers. Pierson and Moskowitz (1964) produced the now called the P-M spectrum. They postulated that given enough time (roughly 10,000 wave periods), a steady wind would come to an equilibrium with waves, defining a "fully developed" sea. To obtain their spectrum of a fully developed sea, they used accelerometers on British weather ships in the North Atlantic. Experiments conducted later in the North Sea (in German Bight) led Hasselmann et al. (1973) to develop a fetch-limited and time-variant spectrum known as the JONSWAP spectrum, rejecting the idea of a "fully developed sea". Though the Bight concerned is only about 20 m deep, the JONSWAP is termed a deep water spectrum because the wavelengths used for measurement were relatively small. Another spectrum, the TMA spectrum was proposed by Bouws et al. (1985) building on the work by Kitaigordskii et al. (1975). The TMA spectrum is a modified version of the JONSWAP spectrum, albeit for water of finite depth. The advantage of the JONSWAP spectrum is that it represents a young sea state, and is thus more common than the "fully developed" sea (Holthuijsen, 2007). The expression for the JONSWAP spectrum is:

$$E(f) = (2\pi)^{-4}\alpha g^2 f^{-5} \exp\left[\frac{-5}{4}\left(\frac{f}{f_m}\right)^{-4}\right]\Gamma(f), \tag{1}$$

where f is the frequency (inverse of wave period), $\Gamma(f)$ is the JONSWAP-peak enhancement function given as:

$$\Gamma(f) = 3.3^{\exp\left[\frac{-\left(1-\frac{f}{f_m}\right)^2}{2\sigma^2}\right]}, \tag{2}$$

where $\sigma = 0.07$ for $f \le f_m$ and $\sigma = 0.09$ for $f > f_m$, g is the acceleration due to gravity and the parameter f_m is the peak frequency given as:

$$f_m = 3.5\tilde{X}^{-0.33}, \tag{3}$$

where $\tilde{X}$ is the modified fetch parameter given as:

$$\tilde{X} = \frac{gX}{U_{10}^2}, \tag{4}$$

where X is the fetch (m) and U_{10} is the wind velocity (m/s) at 10 m above the sea surface.

The parameter α is the traditional Philip's constant (1961) but now evaluated as a function of the modified fetch parameter:

$$\alpha = 0.076\tilde{X}^{-0.22}, \tag{5}$$

note that the JONSWAP spectrum reduces to the Li et al. (2008) spectrum when γ is equal to 1.0. As the upper cutoff of the JONSWAP spectrum is 1.0 Hz (thus the wave period $T = \frac{1}{f}$ is larger than 1.0 s), it represents only gravity waves, and does not extent into capillary waves whose period is usually less than 0.25 s (Dean and Dalrymple, 1984).

It is important to note that the spectrum is based on the linear wave theory, also known as first-order theory (Dean and Dalrymple, 1984). This is understandable as using higher order theories makes the superposition of more than a few waves extremely complicated (Sharma and Dean, 1981).

Once a spectrum is found, all the hydrodynamic properties could be defined based on it. In particular, the wave amplitude a_i for a given frequency f_i (or wave period $T_i = \frac{1}{f_i}$) could be obtained simply as:

$$a_i = \sqrt{2E(f_i)\Delta \mathrm{f}}, \tag{6}$$

where Δf is the frequency increment.

Using the linear theory, the expression for the water free surface, η, for a set of 'n' waves is:

$$\eta = \sum_{i=1}^{n} a_i \cos(k_i x - \omega_i t + \phi_i), \tag{7}$$

where $\omega_i = 2\pi f_i$ is the radian frequency, $k_i = \frac{2\pi}{l_i}$ is the wave number, l_i is the wave length, and ϕ_i is the (random) phase angle. Eq. (7) indicates that the elevation $z = 0$ represents the Mean Water Level (MWL), which coincides with the Still Water Level (SWL) in deep sea. But the MWL is a theoretical line, and when the water surface (water line in 2D vertical) is above it, one cannot obtain the water velocity between the MWL and the water surface. Boufadel et al. (2006) and (2007) used a second-order Taylor expansion from the MWL to obtain the velocity between the MWL and the water surface above it. The approach was attempted herein but did not lead to correct results, because in irregular seas, the water surface could be much higher than the MWL and it could remain there for a long time. Therefore, extrapolating for large distances (above the MWL) and for long durations lead to numerical errors. For this reason, we used the concept known as Wheeler stretching (Wheeler, 1969).

In the Wheeler stretching method, when the water surface, η, is above the MWL the water kinematics is computed by "stretching" the MWL to the instantaneous water line. The Wheeler stretching gave good agreement with laboratory experiments and has comparable results to the computationally intensive kinematic boundary condition fit method (Forristall, 1985).

Applying Wheeler stretching, for each given wave 'i' the velocity expressions takes the form:

$$u_i = a_i\omega_i e^{k_{in}(z-\eta)} \cos(k_{ni}x - \omega_i t + \varphi_i), \tag{8a}$$

$$w_i = a_i\omega_i e^{k_{ni}(z-\eta)} \sin(k_i x - \omega_i t + \varphi_i). \tag{8b}$$

Note that "z" is negative below the MWL. Thus, the velocity components at any (x, z) location are given by the superposition of the corresponding components due to individual waves as given by Eq. (8a) and Eq. (8b). Thus, one obtains:

$$u_{\text{wave}} = \sum_i u_i \tag{9a}$$

$$w_{\text{wave}} = \sum_i w_i. \tag{9b}$$

2.2. Net water transport

A water "particle" at sea (i.e., a small water mass) exhibits a net forward motion known as the Stokes drift (after its discoverer Stokes who first derived a theoretical description for this drift in 1847, Dean and

Dalrymple (1984)). The drift occurs because the forward displacement due to crest passing over the particle is larger than the backward displacement due to the trough passing over the particle. This drift can be reproduced in particle tracking if one use a second order theory or higher. When using the second-order theory, the Stokes drift was reproduced in the transport study of Boufadel et al. (2006) and (2007). As we are using the first order theory herein, the Stokes drift is not produced and thus needs to be superimposed on the kinematics resulting from first order waves. We elected to use the Stokes drift resulting from the most prevalent wave (i.e., at the peak of the spectrum):

$$u_{MSD} = \frac{4\pi^2 a_m^2}{L_m T_m} e^{\frac{4\pi(z-\eta)}{L_m}}, \tag{10}$$

where L_m, T_m, a_m are the length, period, and amplitude of the wave at the spectrum peak. Note that the Stokes' drift decreases exponentially with depth similar to the instantaneous velocities given by Eq. (8a) and Eq. (8b).

Even when using the first order theory, a small forward net motion of particles occur, and it is known as the Lagrangian drift (Sobey, 2001). This motion is much smaller than the true net motion, closely approximated by the Stokes drift (Dean and Dalrymple, 1984). For regular progressive waves, we found numerically that the Lagrangian drift increases with the wave steepness (i.e., ratio of wave height over wave length), and reaches around 10% of the Stokes drift at the maximum steepness of 14%. This Lagrangian drift is accounted for implicitly in our simulations, but is in general a few percent of the Stokes drift herein.

2.3. Oil transport

The governing equation for the transport of oil in the two-dimensional (vertical slice) water column is the two dimensional advection–diffusion equation (Chao et al., 2001; Boufadel et al., 2006; Boufadel et al., 2007):

$$\frac{\partial C}{\partial t} = -U\frac{\partial C}{\partial x} - W\frac{\partial C}{\partial z} - w_b\frac{\partial C}{\partial z} + \frac{\partial}{\partial x}\left(D_x\frac{\partial C}{\partial x}\right) + \frac{\partial}{\partial z}\left(D_z\frac{\partial C}{\partial z}\right), \tag{11}$$

where C is the concentration of oil (mass per unit volume of water), U and W are instantaneous advection velocities in x and z direction respectively, w_b is the velocity due to buoyancy as oil is lighter than water, and D_x and D_z are turbulent diffusion coefficients.

The solution of Eq. (11) can lead to numerical errors due to the change in the nature of the equation depending on the values of velocities and diffusion coefficients (e.g., Tannehill et al., 1997). This has been well established in oil spill modeling, and for this reason, numerous models use an equivalent formulation, known as the Lagrangian form. Thus, Eq. (11) is commonly written in Lagrangian form as:

$$x_{t+1} = x_t + U_p(x_t, z_t, t)\Delta t, \tag{12a}$$

$$z_{t+1} = z_t + W_p(x_t, z_t, t)\Delta t, \tag{12b}$$

where x_t and z_t are the particle coordinates at any given time index t, Δt is the time step, and U_p and W_p are horizontal and vertical components of the particle's velocity, respectively. They are given by:

$$U_p = U + u_d = u_{\text{wave}} + u_{MSD} + u_d, \tag{13a}$$

$$W_p = W + w_d = w_{\text{wave}} + w_b + w_d, \tag{13b}$$

where u_{wave} and w_{wave} are water velocity components due to waves in the x and the z direction (Eq. (9a) and Eq. (9b)). The term u_{MSD} is the component due to the mean Stokes' drift over a wavelength, and w_b is the component due to particle buoyancy (defined in Eq. (11)), which does not depend on the sea state but on the particle dimension and density. It is given as (see Appendix A):

$$w_b = \sqrt{\frac{4g|\rho_d - \rho_w|D_d}{3C_D\rho_w}}, \tag{14}$$

where w_b is the terminal velocity, g is gravity acceleration, ρ_d is the density of the droplet (oil), ρ_w is the water density, D_d is the droplet diameter, and C_D is the drag coefficient, which depends on the flow regime around the droplet due to its own movement (Zhao et al., accepted). Note that each time a particle was higher than the free surface (given by Eq. (7)), it was placed at the free surface.

The terms u_d and w_d in Eq. (13a) and Eq. (13b) are the velocities due to eddy diffusivity in the x and the z directions, given as:

$$u_d = \frac{R_x\sqrt{2D_x\Delta t}}{\Delta t} \tag{15a}$$

$$w_d = \frac{R_z\sqrt{2D_z\Delta t}}{\Delta t} \tag{15b}$$

where R_x and R_z are normal random variables and D_x and D_z are eddy diffusivities in the x and the z direction. Eq. (15a) and Eq. (15b) has also been used by Al-Rabeh et al. (1989) and Chao et al. (2001) for modeling diffusion under a similar state of sea. Since we would be tracking particles at relatively small time scales (time step less than a second), it is reasonable to assume that the eddy diffusivity is isotropic, that is $D_x = D_z$ (Batchelor, 1970; Monin and Yalgom, 1975; Boufadel et al., 2006).

No currents have been assumed, such as those directly resulting from winds (Eley et al., 1988; Daling et al., 1990); currents at much larger scales than the plume simply displace it, and do not affect its spreading. With the exception of buoyant velocity that depends on the droplet properties, the velocities in Eq. (13a) and Eq. (13b) depend only on the sea state. Thus, it is conceivable that one could define a sea state based on easily measured properties and evaluate the transport of oil.

2.4. Eddy diffusivity

The selection of the value of eddy diffusivity is challenging. Ichiye (1967) using dye tracer studies and interpretations using the Reynolds stress concluded that the eddy diffusivity decreases with depth. Thorpe (1984) postulated that eddy diffusivity increases with depth. Kitaigorodskii (1983) had postulated that due to wave breaking, the 'Law of the Wall' analogy used by Thorpe was inapplicable. That is, because of wave breaking, the decrease of the energy dissipation rate with depth is much faster than that given by the law of the wall. Varlamov et al. (1999) developed a formulation dependent on current and wind speed but independent of depth. We adopt the formulation of Ichiye (1967) because it gives an isotropic eddy diffusivity (i.e., $D_x = D_z = D$) that depends on the sea state and decreases with depth, which seems logical. Thus, by conducting Wheeler stretching, one gets:

$$D = \frac{0.028H_s^2}{T_m}\exp\left(\frac{4\pi(z-\eta)}{\lambda}\right) \tag{16}$$

where T_m signifies the peak wave period (taken from the spectrum), and H_s is the significant wave height, which is the average of the largest

one third of wave heights. For the JONSWAP spectrum, it is given by Özger and Sen (2007):

$$H_s = 0.0163\left(\sqrt{\frac{X}{1000}}\right)U_{10}. \tag{17}$$

As Eq. (16) is empirical, and we aimed to provide a holistic view of the impact of turbulent diffusion, we introduced into Eq. (16) two constants, C_1 and C_2 and we explore their variation. Thus, the modified expression becomes:

$$D = C_1\frac{0.028H_s^2}{T_m}\exp\left\{C_2\left(\frac{4\pi(z-\eta)}{\lambda}\right)\right\} \tag{18}$$

2.5. Background mixing

The eddy diffusivity introduced above depends on wave characteristics, and it indicates that no mixing would occur at sea in the absence of waves. However, it is unreasonable to expect that no mixing at all would occur in the absence of waves. For this reason, we use as background mixing in the upper layer, A vertical diffusion coefficient value of 5.0×10^{-5} m^2/s for deep ocean is suggested by Fennel et al. (2001). Zhou et al. (2005) used a value about 10^{-5} m^2/s. We used a smaller mixing coefficient of 10^{-7} m^2/s for the following reason: Dimensional analysis gives that the displacement due to diffusion is $l=\sqrt{D\cdot t}$ (Karabelas, 1978). Thus, for $D=10^{-7}$ m^2/s and $t=1.0$ s, the droplet moves at the speed of 0.03 cm/s. By taking the density of oil to be 0.90 and assuming that $w_b = \sim 3\times10^{-4}$ m/s, one finds a droplet of diameter 70 μm. This is the size below which droplets dispersed at the water surface remain in the water column and do not float back to the surface (Alun et al., 1995) regardless of the sea state. Therefore, a background diffusion coefficient of 10^{-7} m^2/s produces conditions that are more or less observed synoptically.

2.6. Spatial moments of oil droplets

The Lagrangian particle tracking solution of Eq. (12a) and Eq. (12b) is numerically stable. However, for one to understand the overall behavior, one would need to conduct many simulations and to reduce the results in a way that provides accurate characterization of transport. For this reason, we used a Monte Carlo scheme to represent the ensemble quantities related to the transport of oil droplets (Zheng and Wang, 1999). We also used the method of moments to compute the displacement of the plume centroid and the spreading of the plume (Fischer et al., 1979). These quantities could be considered as upscaled quantities for the plume, and we have used this approach in prior works (Boufadel et al., 2006; Boufadel et al., 2007). The moments can be estimated numerically by the equation:

$$M_{c,q}(t) = \sum_{i=1}^{N} m_i\left(s_{c,i}(t)\right)^q,\quad q=0,\ 1,\ 2. \tag{19}$$

The centroid of the plume in any direction 'c' ($c = x$ or z) is given as:

$$S_c = \frac{M_{c,1}(t)}{M_{c,0}(t)}. \tag{20}$$

The variance in direction 'c' is given as:

$$\sigma_c^2(t) = \frac{M_{c,2}(t)}{M_{c,0}(t)} - \left(\frac{M_{c,1}(t)}{M_{c,0}(t)}\right)^2 \tag{21}$$

where m_i is the mass of an oil particle. Since all particles are assumed to be of equal mass (the value of buoyancy is not varied between individual particles), m_i may be set to 1.0. The spreading coefficient in a direction 'c' (x or z) may be obtained according to:

$$E_c(t) = \frac{1}{2}\frac{d}{dt}\sigma_c^2. \tag{22}$$

2.7. Numerical implementation

The range of frequency of the JONSWAP spectrum was set from 0.005 to 0.95 Hz. The spectrum at 0.95 Hz was only 2% of the maximum. The range was discretized into 200 intervals resulting in a frequency interval:

$$df = \left(\frac{f_{\max}-f_{\min}}{200}\right). \tag{23}$$

Particle tracking was conducted by writing a FORTRAN code to integrate Eq. (12a) and Eq. (12b) using a fourth order accurate Runge–Kutta method (Kreyszig, 1999).

Five hundred oil droplets were placed on the free surface at the start of the simulation time. Nine cases were run in this paper with different values of buoyancy and the parameters of the eddy diffusivity formulation, Eq. (18). The considered cases are reported in Table 1. For every case, 20 simulations with different random seeds were used to vary the phase angles of the component waves and to vary the random numbers assigned to the velocities resulting from the turbulent eddy diffusivity (Eq. (15a) and Eq. (15b)). There was no limit on the downward movement of particles. The transport was simulated for a period of hours. For every time step we recorded the positions of each particle, and another FORTRAN code was employed to compute the centroids, variances and spreading coefficients of the individual plumes using Eqs. (20)–(22).

3. Results

3.1. Irregular waves

Wind speed was assumed to be 10 m/s and the fetch was assumed equal to 50 km, which gives a significant height H_s (Eq. (17)) of ≈1.15 m. Table 1 reports the cases that were considered herein, which include four cases (Case 1 through Case 4) with zero buoyancy (i.e., $w_b = 0.0$, Eq. (14)) where the parameters C_1 and C_2 in the eddy diffusivity (Eq. (18)) were changed. The other cases show the base case diffusivity parameters ($C_1 = C_2 = 1.0$), and the terminal buoyant velocity was assigned four values: 4.0×10^{-4}, 1.5×10^{-3}, 5.0×10^{-3}, and 1.0×10^{-2} m/s. A final case was conducted with $C_1 = 0.1$ and the maximum terminal rise (buoyant) velocity of 0.01 m/s.

Fig. 1 shows the free surface and velocity distribution below irregular waves generated by JONSWAP spectrum. The superposition of waves significantly extended the range of the free surface fluctuations. For example, the wave range (i.e., between peak and trough) was around

Table 1
Cases considered based on the coefficients of the diffusion coefficient (Eq. (18)) and the buoyancy velocity (Eq. (14)).

Case	C_1	C_2	Buoyancy velocity w_b, m/s
1	1.0	1.0	0
2	1.0	0.1	0
3	0.1	1.0	0
4	0.1	0.1	0
5	1.0	1.0	4.0×10^{-4}
6	1.0	1.0	1.5×10^{-3}
7	1.0	1.0	5.0×10^{-3}
8	1.0	1.0	1.0×10^{-2}
9	0.1	1.0	0.01

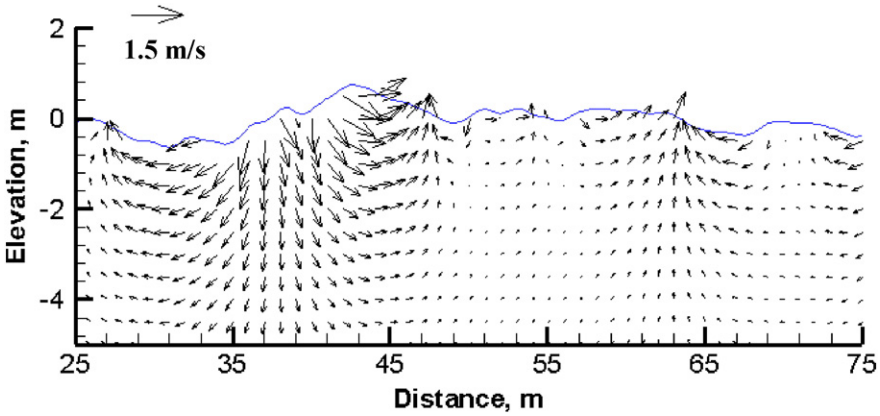

Fig. 1. The free surface and velocity distribution below irregular waves generated by JONSWAP spectrum at $t = 1$ h.

1.5 m between $x = 40$ m and $x = 50$ m. The maximum forward velocity was at the crest and the maximum backward velocity was at the trough, as expected. Moving deeper, the velocity tended to be smaller in general, but there are regions where large velocity values persist with depth, such as at $x = 40$ m. These are most likely due to long waves because the velocity decreases exponentially with depth as given by the term $e^{k_i z}$ in Eq. (8a) and Eq. (8b). Thus, if the wave length is large, k_i is small, and the decrease with depth becomes very small.

3.2. Oil plume movement

The particle plumes are reported in Figs. 2 and 3 for Case 1 and Case 9, respectively. The plumes at $t = 1.0$ h show a "wavy" spatial distribution of particles, reflecting the water profile. But at latter time, the scatter plots seem to lose the "memory" of the initial distribution, and the particles within the plumes appear to be more random. The plumes moved downward with time. The large downward transport was for Case 1 and the small downward transport was for Case 9, as could be deduced visually (a more accurate metric, the plume's centroid is used later in the paper). The downward motion in these graphs is not due to downward velocities due to waves, rather to the movement of the free surface. As we placed all the particles at $z = 0.0$, when the water surface drops below 0.0, it transported the particles downward with it. However, when it rose, it transported only a fraction of them due to turbulent diffusion that moves particles in all direction, including that opposing advection. In other words, for neutrally buoyant particles, when the water surface drops, for example, to −1.0 m depth, the particles continue to behave as if they were placed at $z = -1.0$ m.

All the plumes exhibit the "comet" shape whose front is higher than the tail, especially at latter times. This is due to the Stokes drift, which is largest near the surface and decreases with depth. Thus, particles near the surface move forward faster than deeper particles. This behavior was noted by Elliot et al. (1986) while conducting field studies, and Boufadel et al. (2006) and (2007) while conducting numerical studies of regular waves.

3.3. Effect of eddy diffusivity

Fig. 4a reports the vertical location of the plume's centroid for Case 1 through Case 4, where there was no buoyancy (i.e., $w_b = 0.0$ in Eq. (14)) but the turbulent diffusivity (Eq. (18)) was changed. Case 2 ("base case" magnitude of the diffusion coefficient at $z = 0$ but a small decrease with depth, see Table 1) resulted in the largest drop in the vertical location of the centroid. Case 3 (10% of the magnitude of the "base case" at $z = 0$, and a decrease with depth equal to that of the base case) resulted in the smallest drop in the vertical location of the centroid. For Case 4 (10% of the magnitude of the "base case" diffusion coefficient at $z = 0$ and a small decrease with depth), the centroid z location was above that of the base case for times less than 1.0 h, and below that of the base case at latter times.

Fig. 4b reports the horizontal location of the plume's centroid for Case 1 through Case 4, which should be interpreted based on the results

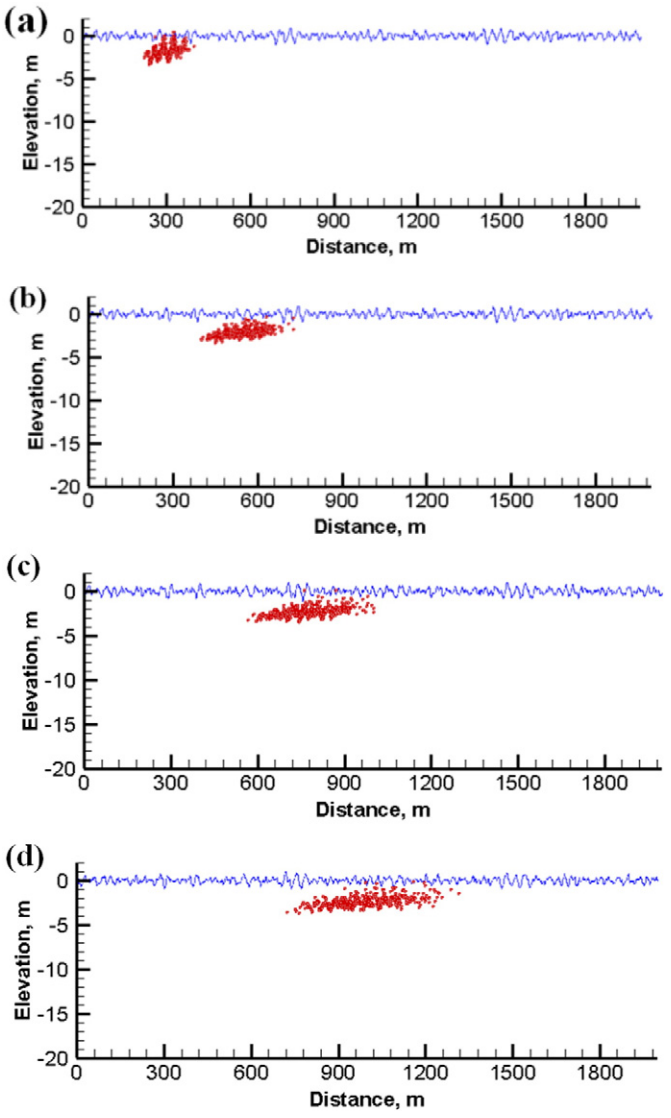

Fig. 2. Particle positions at different time points under irregular wave condition for Case 1: (a) $t = 1$ h; (b) $t = 2$ h; (c) $t = 3$ h; (d) $t = 4$ h.

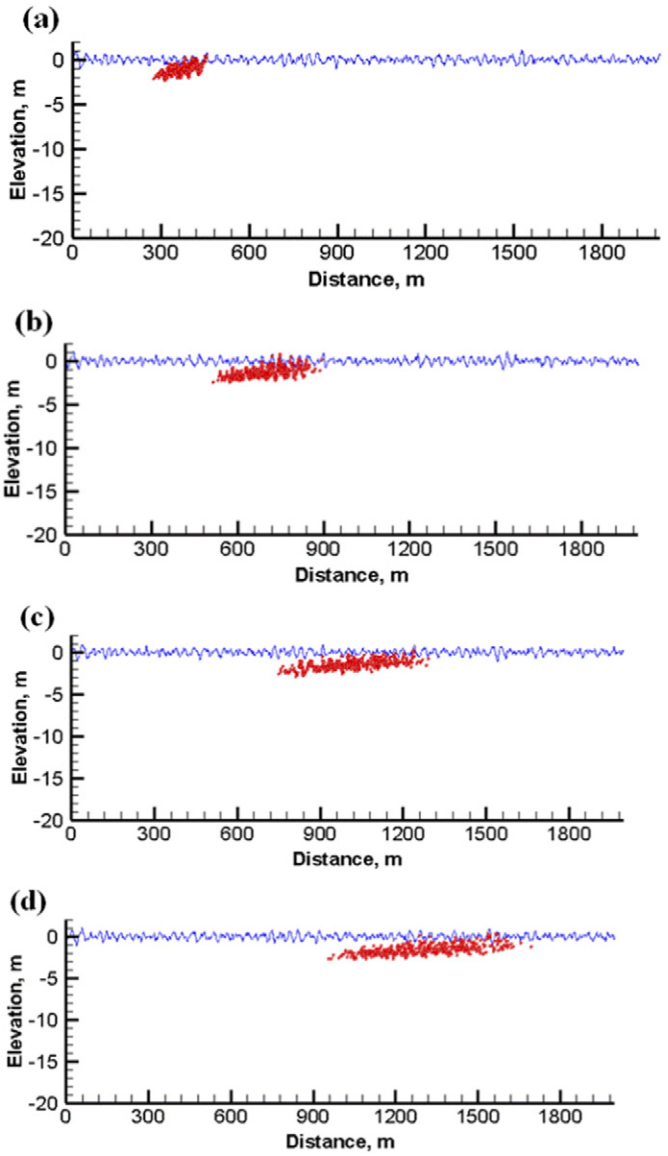

Fig. 3. Particle positions at different time points under irregular wave condition for Case 9: (a) $t = 1$ h; (b) $t = 2$ h; (c) $t = 3$ h; (d) $t = 4$ h.

in Fig. 4a; due to Stokes' drift, the higher the centroid of the plume, the more it moved forward. Conversely, plumes with deep centroid moved forward the least. This is clearly noted for Case 2, which has the smallest centroid elevation, and it had the smallest horizontal displacement. In contrast, Case 3 which has the highest elevation (in terms of centroid location, Fig. 4a), had the largest horizontal displacement.

Fig. 5a depicts how the z-variance of the plume changes with time for various values of the eddy diffusivity. Case 2, which had the largest vertical displacement (Fig. 4a) had also the largest variance. It was followed by Case 4, whose vertical transport (Fig. 4a) was second to that of Case 2. However, Cases 1 and 3 gave the same z-variance, which is probably due to the fact that the curves of their centroids' elevation (Fig. 4a) were parallel to each other, a few minutes after the onset of the simulation.

Fig. 5b depicts how the x-variance of the plume changes with time for the four cases. Case 4 (10% of the magnitude of the "base case" diffusion coefficient at $z = 0$ and a small decrease with depth) resulted in the largest horizontal variance at times larger than 1.0 h. It is because that the eddy diffusivity in Case 4 was largest due to smaller the exponential form C_2 (in comparison to Case 1 and Case 3) and higher plume centroid z_c (in comparison to Case 2).

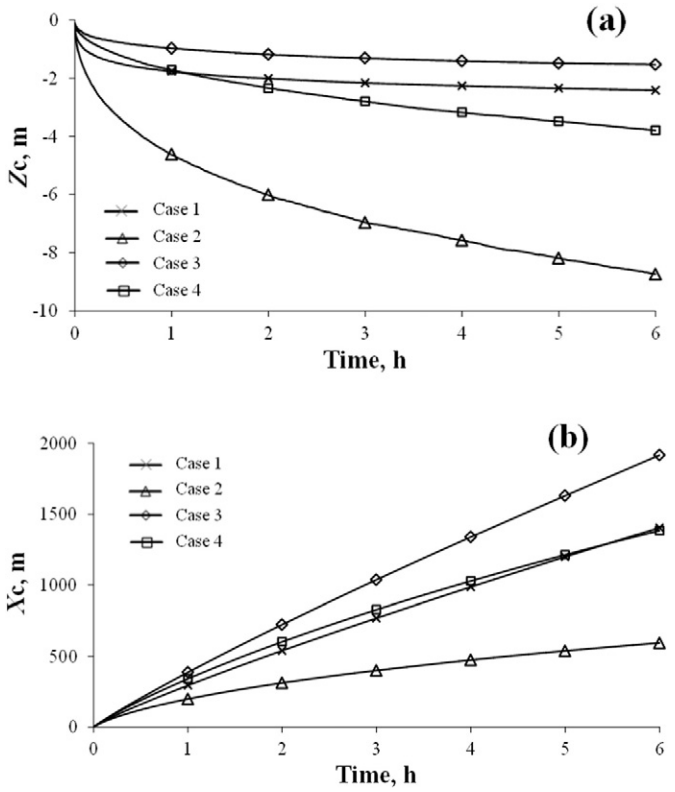

Fig. 4. (a) Vertical location (Z_c) and (b) horizontal location (X_c) of the plume centroid for Case 1, Case 2, Case 3, and Case 4 (Table 1).

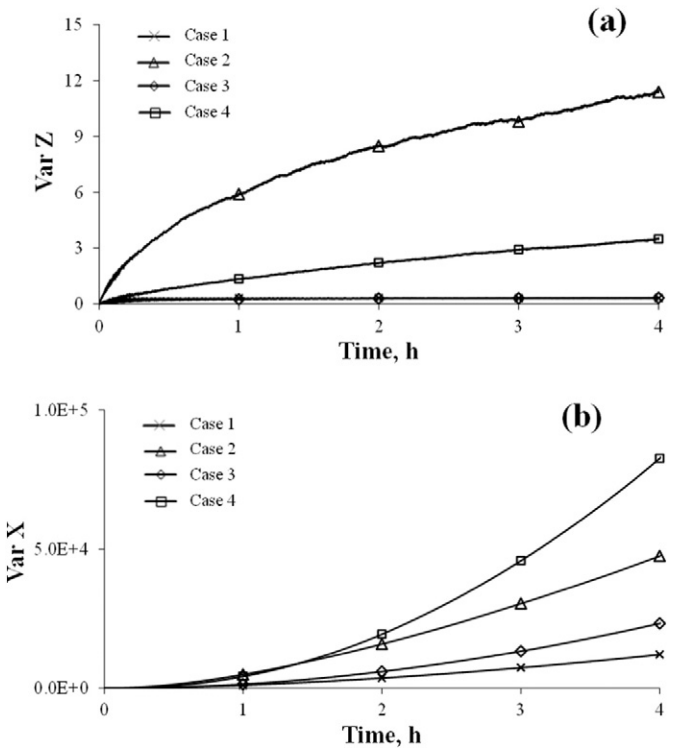

Fig. 5. (a) Vertical variance (σ_z^2) and (b) horizontal variance (σ_x^2) of the plume centroid for Case 1, Case 2, Case 3, and Case 4 (Table 1).

3.4. Effect of buoyancy

We present herein the variation of centroids and variances as function with time for four buoyancy velocity values (w_b). For a given oil, the rise velocity values would represent different particle sizes. However, they could also represent the same size for oil that is weathered and has portions of different density. More generally, as the results stem from superposition, one could combine the findings to obtain the behavior of oils of various properties, as done by Boufadel et al. (2006).

We considered four different rise velocities: 4×10^{-4} m/s, 1.5×10^{-3} m/s, 5.0×10^{-3} m/s, and 1.0×10^{-2} m/s, which for an oil density of 900 kg/m^3 corresponds to spherical particle diameters of 100 μm, 200 μm, 400 μm, and 600 μm.

Fig. 6a and b depicts how the vertical and horizontal locations of the centroid of the plume changes with time for various values of buoyancy. Also shown are the results of the neutrally buoyant case (Case 1) for comparison. Fig. 6a shows that increasing the rise velocity resulted in higher plume's centroid, which is to be expected. The centroid elevation for rise velocities of 5×10^{-3} m/s and 1.0×10^{-2} m/s was practically unchanged, even for larger rise velocity values (not reported). Notice that for the buoyant plumes (i.e., $w_b > 0$), the vertical location of the centroid reached a constant value within half an hour, while the centroid of the neutrally buoyant plume continued to drop with time.

Fig. 6b shows as the buoyancy increased, the horizontal displacement of the plume's centroid increased, which is due to the fact that the Stokes drift is largest at the water surface and decreases with depth, as noted earlier. The plots of the buoyant plumes are straight lines in Fig. 6b because the depth of the plume was constant (Fig. 6a). The vertical and horizontal locations of the neutrally buoyant plume seem to evolve with time in a nonlinear fashion that suggests a decrease in the horizontal displacement with time.

Fig. 7a depicts how the z and x variances of the plume respond to changing values of buoyancy. It is observed that the vertical variance increased with decreasing buoyancy, which is due to the fact that a large buoyancy value brings all the particles close to the surface and thus their vertical range of spreading decreases. This was also noted by Boufadel et al. (2006) while dealing with regular waves. The fluctuations in the neutrally buoyant plot reflect that the particles in that case are more affected by wave kinematics than the buoyant cases. However, all variance values in Fig. 7a are too small to be meaningful in a practical way; in a sea state where the significant wave height, H_s, is ≅1.15 m, a vertical variance of less than 0.3 m^2 (Fig. 7a) gives a vertical standard deviation of $\leq \sqrt{0.3} \cong 0.6$ m, which is almost half of the significant wave height, and thus within the vertical variability of particles due to waves.

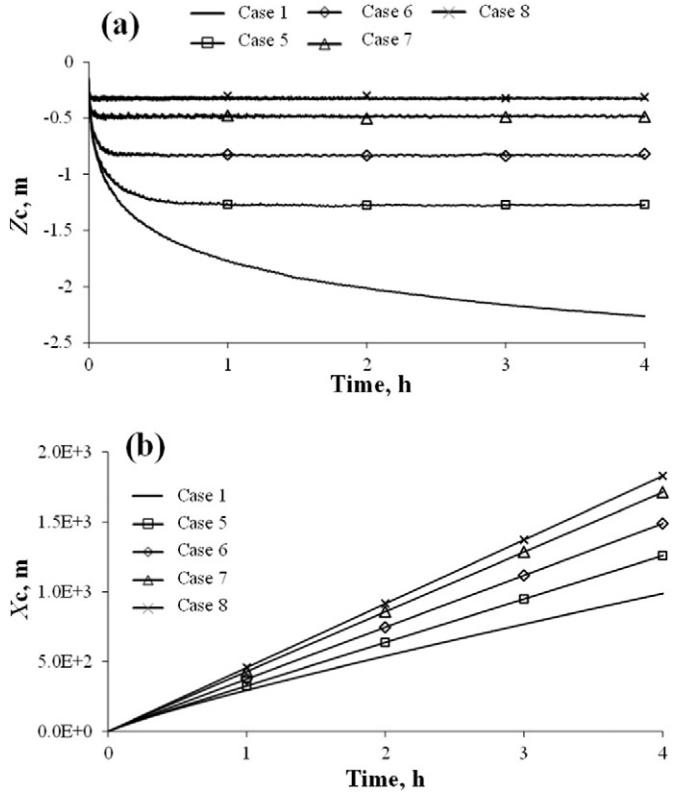

Fig. 6. (a) Vertical location (Z_c) and (b) horizontal location (X_c) of the plume centroid for Case 1, Case 5, Case 6, Case 7, and Case 8 (Table 1).

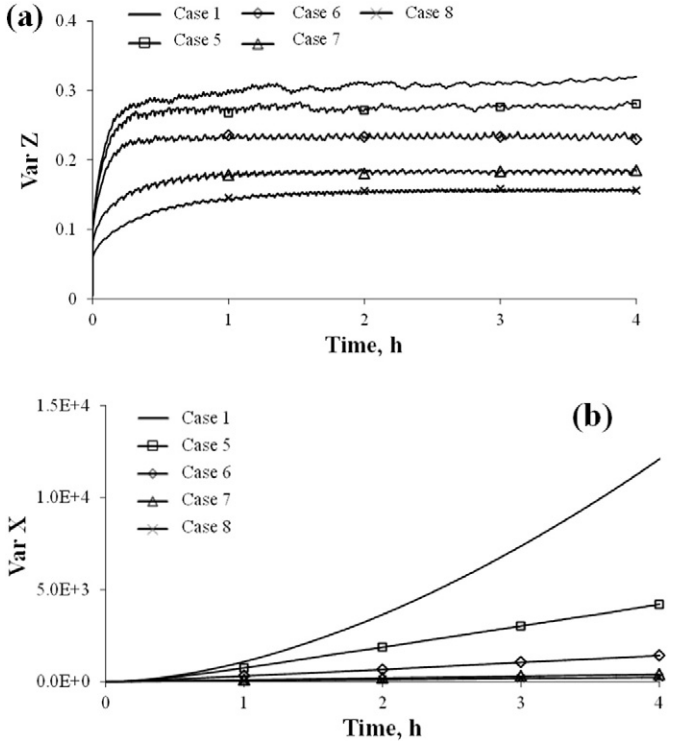

Fig. 7. (a) Vertical variance (σ_z^2) and (b) horizontal variance (σ_x^2) of the plume centroid for Case 1, Case 5, Case 6, Case 7, and Case 8 (Table 1).

Fig. 7b shows that the horizontal variance increased inversely with buoyancy. This is because an increase in buoyancy caused a decrease in the vertical variance (Fig. 7a), and because the major mechanism for horizontal spreading is the variation of Stokes' drift with depth, a small vertical variance (i.e., the plume is more compact in the vertical direction) results in a small horizontal variance. Thus, the horizontal variance depends almost exclusively on the vertical distribution of particles. It follows that higher buoyancy cases would yield minimum horizontal variances.

3.5. Spreading coefficient

Fig. 8a depicts temporal variations of horizontal spreading coefficients of the neutrally-buoyant ensemble plume for varying diffusivity (i.e., Cases 1–4). For varying diffusivity cases, the horizontal spreading coefficients tended to increase with time, after the 4 h of the simulation time, a maximum horizontal spreading coefficient of 5.7 m^2/s for Case 4 appeared. Values ranged in the vicinity of 0.7 m^2/s and 2.5 m^2/s for other diffusion cases. Fig. 8b depicts temporal variations of horizontal spreading coefficients for varying buoyancy cases (i.e., Case 1 and Cases 5–8). It is observed that the horizontal spreading coefficient tended to be smaller for larger size droplets (i.e., larger buoyancy velocity). Apparently, the horizontal spreading coefficient is dependent of the variation of Stokes'

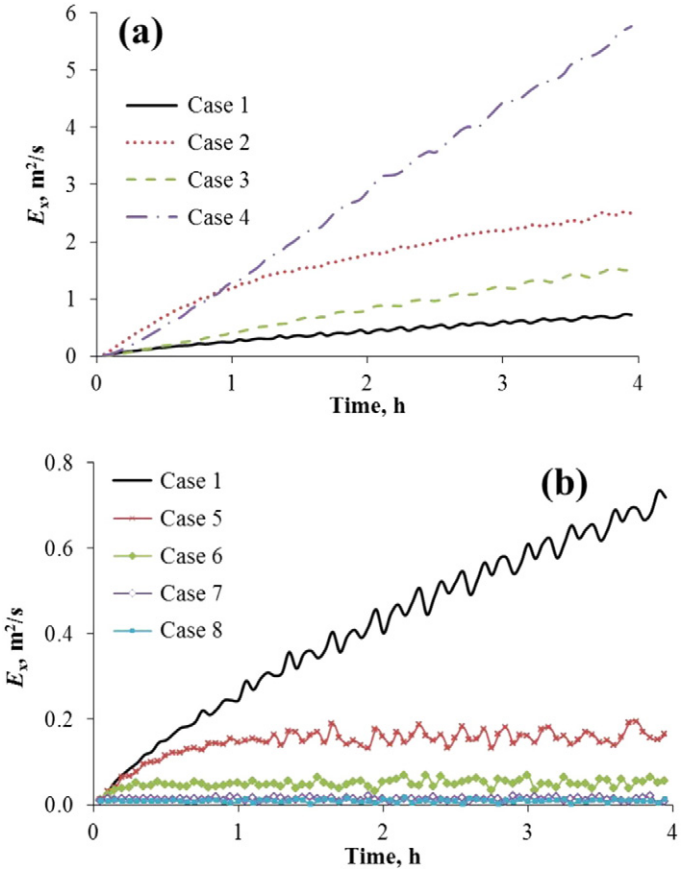

Fig. 8. Horizontal spreading coefficient (E_x) of the plume centroid as a function of time for (a) diffusivity cases (Case 1, Case 2, Case 3, and Case 4) and (b) buoyancy cases (Case 1, Case 5, Case 6, Case 7, and Case 8).

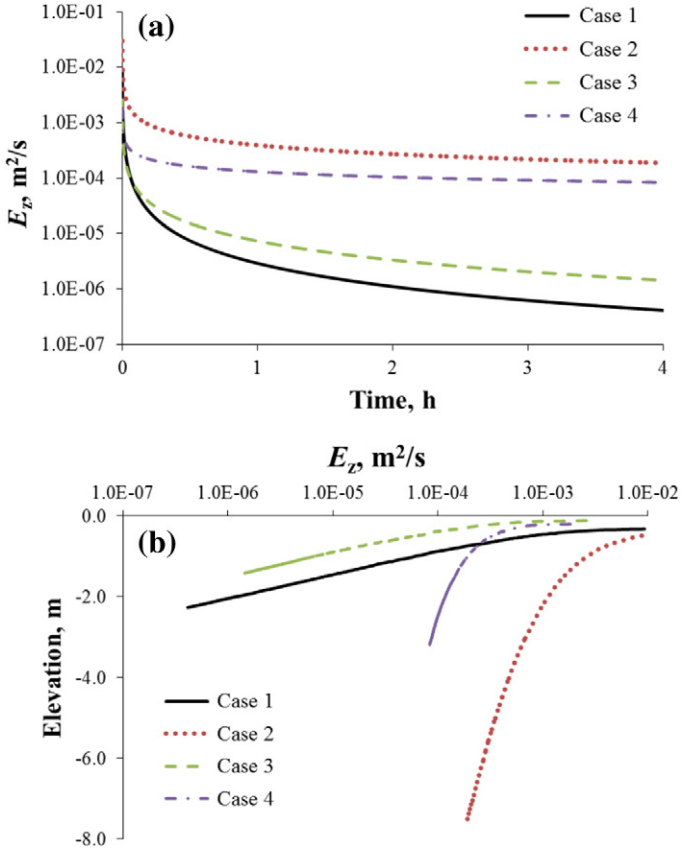

Fig. 9. Vertical spreading coefficient (E_z) of the plume centroid as a function of (a) time and (b) depth for cases where the eddy diffusivity was changed (Case 1, Case 2, Case 3, and Case 4). Note the logarithmic scale.

drift with depth. The larger size droplets are closer to the sea surface and have less downward expansion. Thus, the horizontal spreading tends to be less for the cases with larger buoyancy velocity. Compared to the horizontal direction, the plume had much less spreading in vertical direction. As the vertical spreading coefficient is very small, randomness of Monte Carlo framework might "chaos" the results numerically solved from Eq. (22). In order to obtain more accurate results, the vertical spreading coefficient was obtained by the following steps: the variance of the plume centroid was first fitted by analytical expression, and the spreading coefficients were then directly solved from the analytical expression based on Eq. (22). The fitting results were shown in Fig. S1. The value of coefficient of determination R^2 was more than 0.96 for all the fittings, which suggests that the proposed relation captures closely the temporal response of the centroid variance to irregular waves. Fig. 9a shows the vertical spreading coefficient of the neutrally-buoyant ensemble plume for varying diffusivity (i.e., Cases 1–4). Owing to the concave parabolic nature of the vertical variance plots, the corresponding vertical spreading coefficients for all the cases decreased dramatically in the first half hour and then decreased gradually, leveling off at 2.0×10^{-4} m²/s, 8.4×10^{-5} m²/s, 1.5×10^{-6} m²/s, and 4.2×10^{-7} m²/s for Case 2, Case 4, Case 3, and Case 1, respectively. As the vertical spreading coefficients for Case 2 and Case 4 are at least one order of magnitude larger than that for Case 1 and Case 3, the exponential form C_2 seems play a more important role in determining the vertical spreading coefficient. It is probably due to the fact that with smaller exponential coefficient C_2, the particles still migrated further downward after 4 h, and hence tended to spread more during the migration. In contrast, the vertical spreading coefficient for buoyancy cases was essentially zero after 4 h as the corresponding vertical variance curves tended to be flat (Fig. 7a). Fig. 9b shows a plot of the vertical spreading coefficient as a function of depth, and one notes that, for most cases, the vertical spreading coefficient decreased greatly as approaching the 2.0 m depth, which is on the order of the significant wave height (1.15 m). Fig. 10 shows the spatial variation of the horizontal spreading coefficient, E_x, for all the cases. The variation with distance was quasi-linear for the non-buoyancy cases (Fig. 10a), but in the presence of buoyancy (Fig. 10b), the coefficients reached constant values that are well defined (consistent with Fig. 8).

4. Discussion

The investigation illustrated the role of turbulent diffusion and buoyancy in the presence of wave motion, including Stokes drift. Each buoyancy value could be viewed as representing a droplet size distribution of a particular oil. Thus, one concludes that lighter oils propagate faster forward (Fig. 6). Alternatively, each buoyancy could be viewed as representing a droplet size, and in such a case, if one needs the full droplet size distribution of an oil, one would need to use the superposition approach of Boufadel et al. (2007), developed while dealing with regular waves. As a rule, higher diffusion caused particles to sink deeper, thereby reducing their forward transport due to Stokes drift. Higher diffusion also resulted in increases in the variances. Four different values of buoyancy have been dealt with. It was seen that beyond a vertical rise velocity of 0.01 m/s the results do not change much.

The spreading of the plumes (i.e., the variances) in either the vertical or horizontal was inversely proportional to the oil buoyancy, with the highest spreading occurring for the neutrally buoyancy plumes. This suggest that the lighter the oil, the less it dilutes in the water column, and the denser the oil, the higher its chance for diluting. It has been well recognized that high density oils have high viscosity, and thus

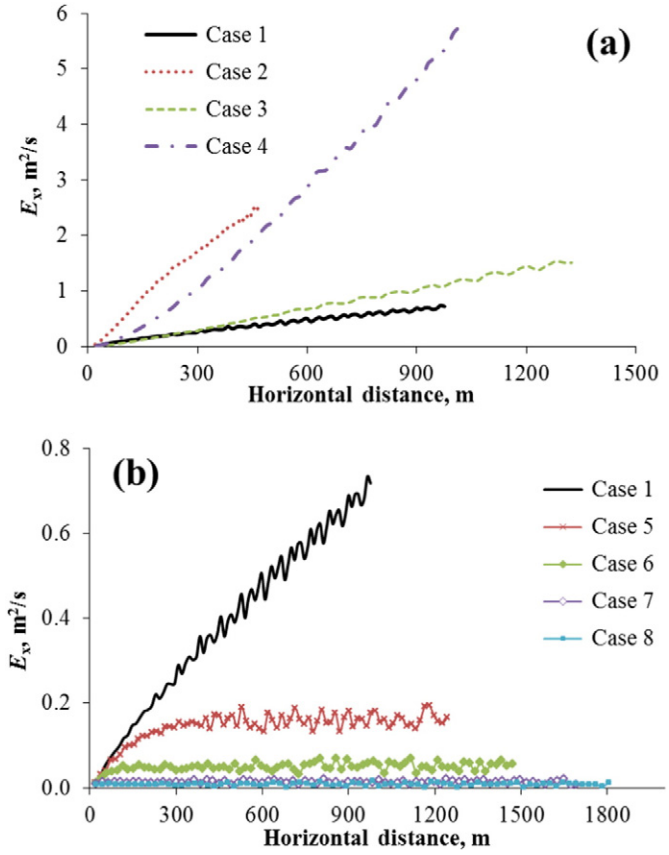

Fig. 10. Spatial variation of horizontal spreading coefficient (E_x) for (a) diffusivity cases (Case 1, Case 2, Case 3, and Case 4) and (b) buoyancy cases (Case 1, Case 5, Case 6, Case 7, and Case 8).

their aqueous toxicity is lower than those of low density oils. The findings herein suggest that not only the chemical property of light oils make them more chemically potent, but their lack of dilution could aggravate their effects. Of course, light oils would evaporate faster than heavy oils, and thus the argument above applies to the buoyancy of oils after the first few hours (or days) of evaporation.

The estimation of the spreading coefficients is arguably the most practical aspect of this work. This is one of the steps needed to upscale the processes occurring at the meter and minutes scales to the scales of kilometers (in the horizontal) and hours, which would be needed for oil models, such as used by Barker (2011), Paris et al. (2012), Poje et al. (2014), and Boufadel et al. (2014).

First it is important to compare our findings to those reported in the literature, as discussed next. For the horizontal spreading coefficient, the value extracted from Okubo's diffusion diagrams (Okubo, 1971) is close to 0.5 m^2/s for a simulation time of 4 h. Csanady (1973) put forward the following analytical expression for estimation of horizontal spreading coefficient:

$$E_x = \frac{1}{2}\frac{ds_1^2}{dt} = a_1 a_2 s_1^{1.33}\varepsilon^{0.33}, \tag{24}$$

where a_1 and a_2 are constants of order unity, s_1 is the plume size and ε is the rate of turbulent energy dissipation (m^2/s^3). For our case herein, we take the plume size as equal to the standard deviation (square root of the variance) of the ensemble plume, which ranges from 15 m to 290 m at 4 h. We assume, based on the significant wave height (0.3 m), that $\varepsilon = 0.01$ m^2/s, which is a reasonable value based on existing works (Drennan et al., 1996), see also short reviews in Kaku et al. (2006a) and (2006b). Eq. (24) then gives a range between 8 m^2/s and 412 m^2/s. Venkatesh et al. (1979) used a value of 10 m^2/s while dealing with surface oil spill in the Bay of Fundy Canada. Elliott and Wallace (1989) presented the following empirical expression for the computation of the horizontal spreading coefficient E_x:

$$E_x = \frac{1.67}{10^4}t^{0.84}, \tag{25}$$

where t is the time in seconds. The value that would result for $t = 4$ h is 0.52 m^2/s. Al-Rabeh et al. (1989) used a value of 10 m^2/s while dealing with surface oil spill occurred in the Abu Ali region on the western side of the Arabian Gulf. Murray (1972) estimated the coefficient to be about 11 m^2/s. The American Society of Civil Engineers (ASCE) Task (1996) reported a value of 10 m^2/s for the Amoco Cadiz spill occurred in the Brittany coast of France at 288 h and a value of 20 m^2/s for the Exxon Valdez spill occurred in Prince William Sound of Alaska (Neff et al., 1995) at 144 h. Modeling the Evoikos oil spill in the Straits of Singapore, Chao et al. (2001) used a value of 7 m^2/s. McCay (2003) addressing the North Cape oil spill, used a horizontal spreading coefficient of 20 m^2/s. French-McCay et al. (2008) conducted a tracer study offshore of San Diego California by releasing a dye on the water surface, and by monitoring its movement using drifters drogued in the mixed layer (estimated to be the top 10 m). They found E_x to vary from less 0.5 m^2 to more than 50 m^2/s. However, a recurrent value was around 10 m^2/s. Barker (2011) used a value of 10 m^2/s for the Gulf of Mexico, which was adopted by Boufadel et al. (2014) in modeling the Deepwater Horizon spill. Overall agreement between Boufadel's simulated results and the deposition of oil on the shorelines, suggests that the value of 10 m^2/s was reasonable. In works of Paris et al. (2012), values of 1 m^2/s and 10^{-5} m^2/s were used for horizontal and vertical eddy diffusivity to simulate the effects of the circulation and synthetic dispersants on the subsea oil transport. Poje et al. (2014) obtained scale-dependent relative diffusivities using high-frequency position data provided by the near-simultaneous release of hundreds of accurately tracked surface drifters. In their study (Fig. 6 in Poje et al. (2014)), the diffusivity was estimated to be 400 m^2/s for the oil plume with 1000 m scale length.

For the vertical spreading coefficient, higher values in the literature come from Venkatesh et al. (1979); Al-Rabeh et al. (1989), and McCay (2003) as cited above, who assumed it to be 0.01 m^2/s. Elliott and Wallace (1989) found the value to be 9.5×10^{-3} m^2/s, while Reed and Gundlach (1989) mentioned it to be 1.0×10^{-3} m^2/s. Matsuno and Wolk (2005) working on experimental spills in the South Japan Sea found it to range from 10^{-6} m^2/s to 10^{-4} m^2/s. Zhou et al. (2005) reported the coefficient to be between 10^{-6} m^2/s to 10^{-2} m^2/s. A value of 10^{-5} m^2/s was reported also by Matsuno et al. (2006). French-McCay et al. (2008) conducted a tracer study offshore of San Diego California by releasing a dye on the water surface, and by monitoring its movement using drifters drogued in the mixed layer (estimated to be the top 10 m). They found vertical spreading coefficient, E_z, to be around 1.0×10^{-3} m^2/s.

The study showed that when using two-dimensional (horizontal) models to predict the movement of surface oil, one would need to use spreading coefficients that account for the buoyancy of the oil in question. Neglecting the buoyancy of oil would overestimate the spreading coefficient, and subsequently the spreading of buoyant oils. The traditional approach of projecting the three-dimensional movement to water flow onto the two-dimensional horizontal plans is well established and has worked well in various applications (see for example Fischer et al., 1979; Rutherford, 1994). However, the buoyancy of the particles adds a fourth parameter, and the problem becomes the projection of a four-dimensional space (as the buoyancy operates independently of any hydrodynamics) onto a two-dimensional space. This usually results in non-uniqueness, whereby multiple combinations produce the same result. Thus, when an oil spill occurs, one would need to estimate the density of the oil after evaporation and dissolution take their toll, and this is

particular important when using a two-dimensional horizontal oil spill model.

The following is the supplementary data related to this article.

Supplementary data to this article can be found online at http://dx.doi.org/10.1016/j.marpolbul.2016.01.007.

Acknowledgment

This research was supported in part through funding from the Department of Fisheries and Oceans Canada under Contract No. F5211-130060. This research paper was made possible, in part, by a grant from The Gulf of Mexico Research Initiative to the Consortium CARTHE II. No official endorsement should be implied from the funding entities.

Appendix A

The rising velocity is calculated based on the correlation formulations for contaminated fluid particles in three size ranges (Clift et al., 1978; Zheng and Yapa, 2000):

1. Small spherical shape ($d_i \le 1$ mm)

$$U_r = \frac{R\mu}{\rho_c d_i} \tag{A1}$$

where μ is the dynamic viscosity of the continuous phase (Pa.s) (i.e., water herein); ρ_c is the density of the continuous phase (kg/m^3); d_i is the bubble diameter (m); R is the Reynolds number whose computational procedure can be found in Zheng and Yapa (2000).

2. Ellipsoidal shape ($1\text{ mm} < d_i \le d_{cr}$)

$$U_r = \frac{\mu}{\rho_c D_e} M^{-0.149}(J-0.857) \tag{A2}$$

where D_e is the equivalent diameter (m), d_{cr} is the critical diameter between ellipsoidal shape and spherical cap shape (discussed later); J is a general correlation which can be expressed as:

$$J = 0.94H^{0.757} \qquad (2<H\le 59.3) \tag{A3}$$

$$J = 3.42H^{0.441} \qquad (H>59.3) \tag{A4}$$

in which

$$H = \frac{4}{3} Eo M^{-0.149}(\mu/\mu_W)^{-0.14} \tag{A5}$$

where μ_w is dynamic viscosity of water, which can be taken as 0.9 cp herein, Eo is Eotvos number, and M is the Morton number, both reflect the shape of the bubble, and are defined as:

$$M = \frac{g\mu^4\Delta\rho}{\rho_c^2\sigma^3} \tag{A6}$$

$$Eo = g\Delta\rho D_e^2/\sigma. \tag{A7}$$

The Eotvos number is a dimensionless number that represents the ratio of buoyancy forces to interfacial forces, and the Morton number represents roughly the ratio of forces deforming the droplet to those keeping it spherical.

3. Spherical cap shape ($d_i > d_{cr}$)

$$U_B = 0.711\sqrt{gD_e\Delta\rho/\rho_c} \tag{A8}$$

The critical diameter d_{cr} can be determined by solving Eqs. (A2) and (A8) simultaneously to get an intersection point, or, considering Eqs. (A2) and (A8) as a straight line in a logarithmic coordinate, one can obtained the point of intersection between the two lines as presented in Zheng and Yapa (2000).

References

Al-Rabeh, A.H., Cekirge, H.M., Gunay, N., 1989. A stochastic simulation model of oil spill fate and transport. Appl. Math. Model. 13, 322–329.

Alun, L., Daling, P.S., Strøm-Kristiansen, T., Nordvik, A.B., Fiocco, R.J., 1995. Weathering and chemical dispersion of oil at sea. Proceedings of International Oil Spill Conference 1. American Petroleum Institute, pp. 157–164.

ASCE Task Committee, 1996. State-of-the-art review of modeling transport and fate of oil spills. J. Hydraul. Eng. 122 (11), 594–609.

Barker, C.H.C.H., 2011. A statistical outlook for the Deepwater Horizon oil spill. Monitoring and Modeling the Deepwater Horizon Oil Spill: A Record-Breaking Enterprise. American Geophysical Union, Washington, D.C., pp. 237–244.

Batchelor, G.K., 1970. The theory of homogeneous turbulence. Cambridge University Press.

Boufadel, M.C., Bechtel, R.D., Weaver, J.W., 2006. The movement of oil under non-breaking waves. Mar. Pollut. Bull. 52, 1056–1065.

Boufadel, M.C., Du, K., Kaku, V.J., Weaver, J.W., 2007. Lagrangian simulation of oil droplets transport due to regular waves. Environ. Model Softw. 22 (7), 978–986.

Boufadel, M.C., Abdollahi-Nasab, A., Geng, X., Galt, J., Torlapati, J., 2014. Simulation of the landfall of the deepwater horizon oil on the shorelines of the gulf of Mexico. Environ. Sci. Technol. 48 (16), 9496–9505.

Bouws, E., Günther, H., Rosenthal, W., Vincent, C.L., 1985. Similarity of the wind wave spectrum in finite depth water. J. Geophys. Res. 90 (C1), 975–986.

Chao, X., Shankar, N.J., Cheong, H.F., 2001. Two-and three-dimensional oil spill model for coastal waters. Ocean Eng. 28, 1557–1573.

Clift, R., Grace, J.R., Weber, M.E., 1978. Bubbles, drops, and particles. Academic Press, San Diego.

Coulaloglou, C.A., Tavlarides, L.L., 1977. Description of interaction processes in agitated liquid–liquid dispersions. Chem. Eng. Sci. 32 (11), 1289–1297.

Csanady, G.T., 1973. Turbulent Diffusion in the Environment (Geophysics and Astrophysics Monographs). Springer.

Daling, P.S., Mackay, D., Mackay, N., Brandvik, P.J., 1990. Droplet size distributions in chemical dispersion of oil spills: towards a mathematical model. Oil Chem. Pollut. 7, 173–198.

Dean, R.G., Dalrymple, R.A., 1984. Water wave mechanics for engineers and scientists. Prentice-Hall, Inc., New Jersey.

Drennan, W.M., Donelan, M.A., Terray, E.A., Katsaros, K.B., 1996. Oceanic turbulence dissipation measurements in SWADE. J. Phys. Oceanogr. 26, 808–815.

Eley, D.D., Hey, M.J., Symonds, J.D., 1988. Emulsions of water in asphaltene-containing oils 1. Droplet size distribution and emulsification rates. Colloids Surf. 32, 87–101.

Elliot, A.J., Hurford, N., Penn, C.J., 1986. Shear diffusion and the spreading of oil slicks. Mar. Pollut. Bull. 17 (7), 308–313.

Elliott, A.J., Wallace, D.C., 1989. Dispersion of surface plumes in the southern North Sea. Ocean Dyn. 42, 1–16.

Fennel, K., Spitz, Y.H., Letelier, R.M., Abbott, M.R., Karl, D.M., 2001. A deterministic model for N2 fixation at stn. ALOHA in the subtropical North Pacific Ocean. Deep-Sea Res. II Top. Stud. Oceanogr. 49 (1–3), 149–174.

Fischer, H.B., List, E.J., Koh, R.C.Y., Imberger, J., Brooks, N.H., 1979. Mixing in inland and coastal waters. Academic Press, New York.

Forristall, G.Z., 1985. Irregular wave kinematics from a kinematic boundary condition fit. Appl. Ocean Res. 7 (4), 202–212.

French-McCay, D.P., Mueller, C., Payne, J., Terrill, E., Otero, M., Kim, S.Y., Carter, M., Nordhausen, W., Lampinen, M., Ohlmann, C., 2008. Dispersed oil transport modeling calibrated by field-collected data measuring fluorescein dye dispersion. International Oil Spill Conference 1. American Petroleum Institute, pp. 527–536.

Hasselmann, K., Barnett, T.P., Bouws, E., Carlson, H., Cartrwight, D.E., Enke, K., Ewing, J.A., Geinapp, H., Hasselmann, D.E., Kruseman, F., Meerburg, A., Muller, P., Olbers, D.J., Richter, K., Sell, W., Walden, H., 1973. Measurement of wind-wave growth swell and decay during the Joint North Sea Wave Project (JONSWAP). Dtsch. Hydrogr. Z. A8 (12), 1–95.

Holthuijsen, L.H., 2007. Waves in oceanic and coastal waters. Cambridge University Press.

Ichiye, T., 1967. Upper ocean boundary-layer flow determined by dye diffusion. Phys. Fluids Suppl. 10, 270–279.

Kaku, V.J., Boufadel, M.C., Venosa, A.D., Weaver, J.W., 2006a. Evaluation of mixing energy in laboratory flasks used for dispersant effectiveness testing. J. Environ. Eng. ASCE 132 (1), 93–101.

Kaku, V.J., Boufadel, M.C., Venosa, A.D., Weaver, J.W., 2006b. Flow dynamics in eccentrically rotating flasks used for dispersant effectiveness testing. Environ. Fluid Mech. 6 (4), 385–406.

Karabelas, A.J., 1978. Droplet size spectra generated in turbulent pipe flow of dilute liquid/liquid dispersions. AIChE J 24 (2), 170–180.

Kitaigordskii, S.A., Krasitskii, V.P., Zaslavskii, M.M., 1975. on phillips' theory of equilibrium range in the spectra of wind-generated gravity waves. J. Phys. Oceanogr. 5, 410–420.

Kitaigorodskii, S.A., 1983. On the theory of the equilibrium range in the spectrum of wind generated gravity waves. J. Phys. Oceanogr. 13, 816–827.

Korotenko, K., Mamedov, R., Mooers, C., 2000. Prediction of the dispersal of oil transport in the Caspian Sea resulting from a continuous release. Spill Sci. Technol. Bull. 6 (5), 323–339.

Kreyszig, E., 1999. Advanced engineering mathematics. eighth ed. John Wiley & Sons, New York.

Li, Z., Lee, K., King, T., Boufadel, M.C., Venosa, A.D., 2008. Assessment of chemical dispersant effectiveness in a wave tank under regular non-breaking and breaking wave conditions. Mar. Pollut. Bull. 56 (5), 903–912.
Matsuno, T., Wolk, F., 2005. Observations of turbulent energy dissipation rate ε in the Japan sea. Deep-Sea Res. II Top. Stud. Oceanogr. 52, 1564–1579.
Matsuno, T., Lee, J.-S., Shimizu, M., Kim, S.-H., Pang, I.-C., 2006. Measurements of the turbulent energy dissipation rate ε and an evaluation of the dispersion process of the Changjiang Diluted Water in the East China Sea. J. Geophys. Res. 111, C11S09.
McCay, D.F., 2003. Development and application of damage assesment modeling: example assessment for the North Cape oil spill. Mar. Pollut. Bull. 47, 341–359.
Millies, M., Mewes, D., 1999. Interfacial area density in bubbly flow. Chem. Eng. Process. Process Intensif. 38, 307–319.
Monin, A.S., Yalgom, A.M., 1975. Statistical fluid mechanics: mechanics of turbulence. MIT Press, Cambridge, Massachusetts.
Murray, S.P., 1972. Turbulent diffusion of oil in the ocean. Limnol. and Oceanogr 17, 651–660.
Neff, J.M., Owens, E.H., Stoker, S.W., McCormick, D.M., 1995. Shoreline oiling conditions in Prince William Sound following the Exxon Valdez oil spill. American Society for Testing and Materials, Philadelphia, PA (United States).
Okubo, A., 1971. Oceanic diffusion diagrams. Deep-Sea Res. 18, 789–802.
Özger, M., Sen, Z., 2007. Triple diagram method for the prediction of wave height and period. Ocean Eng. 34, 1061.
Paris, C.B., Hénaff, M.L., Aman, Z.M., Subramaniam, A., Helgers, J., Wang, D.P., Kourafalou, V.H., Srinivasan, A., 2012. Evolution of the Macondo well blowout: Simulating the effects of the circulation and synthetic dispersants on the subsea oil transport. Environ. Sci. Technol. 46 (24), 13293–13302.
Phillips, O.M., 1985. Spectral and statistical properties of the equilibrium range in wind-generated gravity waves. J. Fluid Mech. 156, 505–531.
Pierson, W.J.J., Moskowitz, L., 1964. A proposed spectral form for fully developed wind seas based on the similarity theory of S.A. Kitaigorodskii. J. Geophys. Res. 69 (24), 5181–5190.
Pohorecki, R., Moniuk, W., Bielski, P., Zdrójkowski, A., 2001. Modelling of the coalescence/redispersion processes in bubble columns. Chem. Eng. Sci. 56, 6157–6164.
Poje, A.C., Özgökmen, T.M., Lipphardt, B.L., Haus, B.K., Ryan, E.H., Haza, A.C., Jacobs, G.A., Reniers, A., Olascoaga, M.J., Novelli, G., 2014. Submesoscale dispersion in the vicinity of the Deepwater Horizon spill. Proc. Natl. Acad. Sci. 111 (35), 12693–12698.
Reed, M., Gundlach, E., 1989. A coastal zone oil spill model: development and senstivity studies. Oil Chem. Pollut. 5, 411–449.
Rutherford, J.C., 1994. River Mixing. John Wiley and Sons.
Sharma, J.N., Dean, R.G., 1981. Second-order directional seas and associated wave forces. Soc. Petrol. Eng. J. 21 (1), 129–140.
Singleton, 2008. The Beaufort scale of winds — its relevance, and its use by sailors. 63 (2), 37–41.
Sobey, R.J., 2001. Coastal Hydrodynamics.
Sobey, R.J., Barker, C.H., 1997. Wave-driven transport of surface oil. J. Coast. Res. 13 (2), 490–496.
Tannehill, J.C., Anderson, D.A., Pletcher, R.H., 1997. Computational fluid mechanics and heat transfer. Hemisphere Publishing, Philadelphia.
Thorpe, S.A., 1984. A model of turbulent diffusion of bubbles below the sea surface. J. Phys. Oceanogr. 14, 841–854.
Varlamov, S.M., Yoon, J.-H., Hirose, N., Kawamura, H., Shiohara, K., 1999. Simulation of the oil spill porcesses in the sea of Japan with regional ocean ciculation model. J. Mar. Sci. Technol. 4, 94–107.
Venkatesh, S., Sahota, H., Rizkalla, A., 1979. Prediction of the motion of oil spills in Canadian arctic waters. International Oil Spill Conference 1979(1). American Petroleum Institute, pp. 677–683.
Walter, J.G., Blanch, H.W., 1986. Bubble break-up in gas–liquid bioreactors: break-up in turbulent flows. Chem. Eng. J. 32 (1), B7–B17.
Wang, S., Shen, Y., Zheng, Y., 2005. Two-dimensional numerical simulation for transport and fate of oil spills in seas. Ocean Eng. 32 (13), 1556–1571.
Wheeler, J.D., 1969. Method for calculating forces produced by irregular waves. Offshore Technology Conference 22(3), pp. 71–82.
Zhao, L., Boufadel, M.C., Lee, K., King, T., Loney, N., Geng, X., 2016. Evolution of bubble size distribution from gas blowout in shallow water. J. Geophys. Res. (accepted).
Zheng, C., Wang, P.P., 1999. MT3DMS-A modular three-dimensional multispecies transport model for simulation of advection, dispersion and chemical reactions of contaminant in ground-water systems: Documentation and user's guide. Contract Rep. SERDP-99-1, U.S. Army Eng. Res. and Dev. Cent., Vicksburg, Miss.
Zheng, L., Yapa, P.D., 2000. Buoyant velocity of spherical and nonspherical bubbles/droplets. J. Hydraul. Eng. 11 (852), 852–854.
Zhou, L., Tian, J., Zhang, X., 2005. Observation of small-scale processes over shelf break in the East China Sea. Chin. Sci. Bull. 50 (24), 2885–2890.